J Intell Robot Syst (2008) 52:79–99
DOI 10.1007/s10846-008-9204-y

Vehicle Simulation System: Controls and Virtual-reality-based Dynamics Simulation

Elvedin Kljuno · Robert L. Williams II

Received: 24 July 2007 / Accepted: 9 January 2008 /
Published online: 16 February 2008

Abstract This paper introduces a cable-suspended robot, the vehicle simulation system, designed for pilot and driver training. The main idea of this work is to make a system that will provide realistic simulations of vehicle motion using virtual reality and a motion platform. A method to produce inertial forces acting on the vehicle user is proposed. A detailed description of the robot's dynamics constraints is provided, accompanied with a numerical solution. Using the developed mathematical model, the robot workspace is analyzed, as well as the influence of the end-effector orientation angle ranges on the available workspace. Adequate robot platform motion is provided through four control systems in a form of a cascade control with a fuzzy logic controller in outer loops. The cable robot is non-linear and difficult from a classical control point of view, since it requires a local linearization of the dynamics equations. A fuzzy logic control concept has been applied in order to control the end-effector position, velocity and acceleration and it turns out to be convenient in simulation, allied with inner-loop classical control. As the system is under-constrained, with nine unknown cable tensions and six dynamics equations, an optimization method is used. The control complexity is increased by the requirement, specific to cable robots, of maintaining positive cable tensions. The system simulations are done using a virtual reality environment and results are presented accompanied with the discussion.

Keywords Vehicle simulation system · Cable robot · Cable tension · Workspace · Kinematics · Dynamics · Virtual reality motion simulation · Fuzzy logic control

E. Kljuno
Department of Mechanical Engineering, University of Sarajevo, Vilsonovo Setaliste 9, 71000 Sarajevo, Bosnia and Herzegovina
e-mail: ek289806@ohio.edu

R. L. Williams II (✉)
Department of Mechanical Engineering, Ohio University, 259 Stocker Center, Athens, OH 45701-2979, USA
e-mail: williar4@ohio.edu
URL: http://www.ent.ohiou.edu/~bobw

1 Introduction

Flight simulators have been in use since the 1960s, generally constructed of a heavy, hydraulically-driven Stewart Platform variant and very special purpose. The innovation in this article is to replace the Stewart Platform with a lighter, more economical, possibly safer cable-suspended robot with a much better payload-to-weight ratio. Also, a main feature is that the real-world cockpits of a variety of vehicles may be used in VR simulation with realistic vehicle motion: aircraft, automotive, mountain biking, horse riding, kayaking, surfing, skiing, etc. Our literature search revealed few similar works. Usher et al. [9] present a cable-suspended robot to aid in controls development for an autonomous helicopter. Marshall [4] describes a three-mile-long cable array to be used for UAV operator training.

First-time experience with an aircraft or a helicopter can be stressful due to high inertial forces acting on pilots. Use of a simulator for pilots training is a regular practice. Such simulators already exist in the form of parallel robot structures with hydraulic actuators. However, the idea proposed in this paper is to use a cable robot in a form of a vehicle simulation system (Fig. 1). We term this Whole-body Haptics, wherein the human operator rides in a realistic cockpit, with VR vehicle motion simulation and feels the inertial forces of motion due to the simulated motion.

The main benefits of a cable robot application is very high ratio external load/robot weight, low inertial forces acting on the robot structure, and the possibility to obtain very high end-effector accelerations, due to relatively low mass of the robot structure. However, the advantages in mechanical structure are somewhat shadowed with significant increase in complexity of the robot control concept. The main obstacle is the fact that a cable cannot transfer the compression forces. Moreover, the complexity of the control is reflected in the fact that a cable robot is highly non-linear object and complex for classical control application.

Most cable robots research done in the past is related to determination of a cable robot workspace for various static loads of end-effectors. An analytical approach to define the workspace for a robot with 6 cables, loaded with an arbitrary wrench acting on the end-effector, is given in Bosscher et al. [3]. Other analyses of cable robot workspace are done by developing the governing equations analytically and then solving them numerically [6, 7].

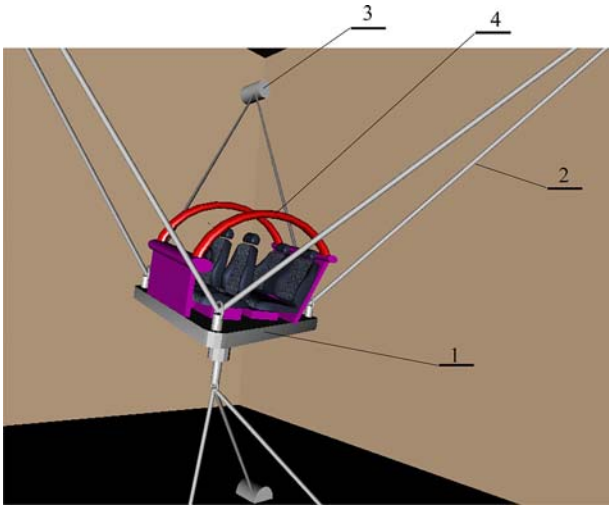

Fig. 1 Vehicle simulation system: *1* platform, *2* cables, *3* actuators, *4* cockpit

In general, a cable robot has an end-effector that has 6 *df* for 3D motion, or 3 *df* for a planar motion. This means that it is possible to establish six differential equations (or algebraic, if a pseudo-static case is considered) in the 3D case or three equations in the 2D case. On the other hand, a cable robot can have an arbitrary number of cables and each cable introduces a new unknown variable that should be determined by a dynamics analysis. To obtain a solution in a case that there are more unknown cable tensions than dynamics equations, some kind of optimization method has to be applied. Some of those methods are described in Williams et al. [11]; Park et al. [5]; and Williams and Gallina [12].

A particular task of a cable-robot requires a particular motion defined in Cartesian coordinates with specified position and orientation, and/or velocity, and/or acceleration of the end-effector. However, the variables that can be directly controlled are cable tensions, via motor torques that cables are connected to. Some information about cable-robot control using a classical feedback control approach can be found in Yingjie et al. [13] and [8].

2 Vehicle Simulation System (VSS) Concept

Figure 2 presents the new concept for a Whole-body Haptics Vehicle Simulator System (VSS). The 6-*df* (*xyz* translations, roll-pitch-yaw rotations) motion for the human user is imparted using the ceiling-mounted six-cable-suspended robot. The rotations are rather limited, similar to a Stewart–Gough Platform, but the translational workspace can be quite large with a cable-suspended robot. Motors and cable reels are fixed to the ceiling and floor and the cable ends are attached to the moving platform carrying the vehicle cockpit. The system bandwidth and accelerations will be designed to allow a variety of vehicle simulations. The cockpit is the real device from the real world, insofar as possible, including real input devices for realism. We will include haptic (force-feedback) inputs where possible such as haptic flight sticks or haptic driving wheels. As shown in Figs. 1 and 2, the cable robot is a modified NIST RoboCrane [1], which itself is a 3–3 Stewart–Gough platform inverted and hung from the ceiling, with active cables in place of hydraulic cylinder legs. We modify the RoboCrane to include three cables pulling down from the floor (see Figs. 1 and 2) for crisp downward motions. That is, in this way we needn't rely on gravity for downward accelerations (plus, downward accelerations larger than g can be achieved in this manner). The redundant down-pulling cables convert the gravity-constrained RoboCrane to a fully constrained cable robot.

The platform has a 100-kg mass and equilateral triangular shape. The role of this platform within the cable robot is to bear a cockpit together with a driver and necessary equipment for manual and automatic control to simulate various vehicle motions. There are nine steel cables of a proper size (10 mm) tied to the platform and actuators. The VSS includes nine electrical DC motors that are used to move and position the platform by pulling the cables. The actuators are positioned in pairs at the top of the workspace in corners of the equilateral triangle of side 4 m. Besides six actuators positioned at the top of the workspace, there are three additional actuators at the bottom in the corners of the equilateral triangle of 1 m side. The cockpit provides seats with safety equipment and equipment for measurement, manual control, and automatic control of the platform motion. The cockpit must provide complete protection from cable interference with the driver and the equipment. The 4×3 m screen is used to show a realistic motion through a particular environment (a car road, an airplane path, a helicopter path, etc.).

Motors can increase or decrease the cable lengths. In this way, the platform can be positioned to the desired point and attitude within the robot workspace. By controlling

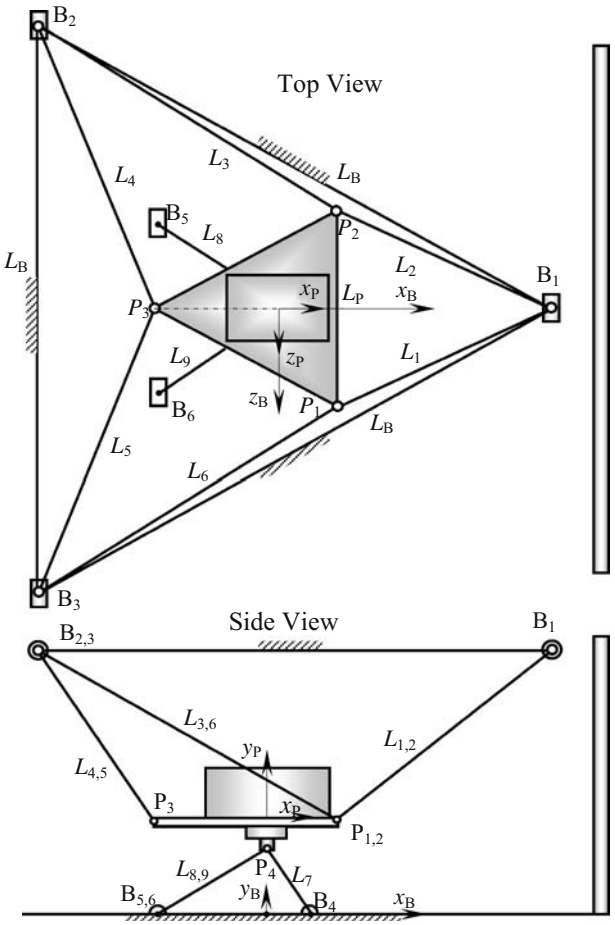

Fig. 2 Vehicle simulation system diagram

cable velocities, desired Cartesian vectors of linear and angular platform velocity at every position can be obtained. Besides the velocity control, in similar way a desired angular and linear acceleration of the platform can be obtained.

The idea proposed in this paper is to assemble the vehicle simulation system in front of a large screen (Fig. 3) and simulate a motion through a desired environment to a pilot/driver in the cockpit by using proper visual effects and simultaneously produce inertial forces acting on the user proportional to those that would appear in real motion through that particular environment, to enhance operator training and experience.

The existence of adequate inertial forces acting on the driver is important to make the simulation realistic. To simulate a military airplane motion, VSS has to produce very high acceleration perpendicular to the motion path. Due to the limited workspace of the system, any acceleration in a particular direction cannot last too long, but there are existing methods in the industry to address this. Figure 4 shows a view from the cockpit onto the screen during a virtual reality motion simulation.

The forward and inverse kinematics equations for the vehicle simulation system have been presented in Williams [10]. In order to design a control system that will provide an

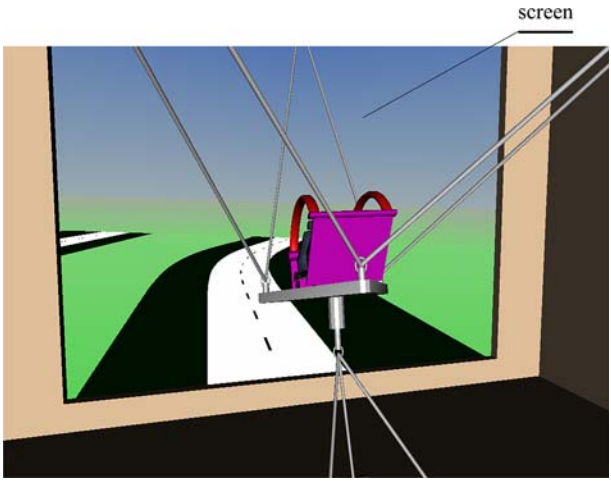

Fig. 3 Vehicle simulation system positioned in front of a screen

adequate motion of the platform corresponding to the simulated motion on the screen, the robot dynamics equations must be derived.

The VSS may be used in two types of simulations: (1) Passive, where the trainee or user just enjoys some realistic motions while watching realistic graphical simulations of the motions. This is useful in the early training stages or for passive entertainment. (2) Active, wherein the trainee or user moves the input device (such as flight stick or automotive steering wheel) to cause the platform to move and thus feel the dynamics of their vehicle control actions, for more meaningful real-world training in the VR environment.

In either mode the view on the screen currently changes with the vehicle motion. That is, under either passive or active vehicle motions, the view provided automatically to the users is from a virtual camera mounted to the simulated vehicle. An alternative to this will be developed in the future, i.e. the view should change to match not only the vehicle motion, but the primary user's head motions, for increased realism.

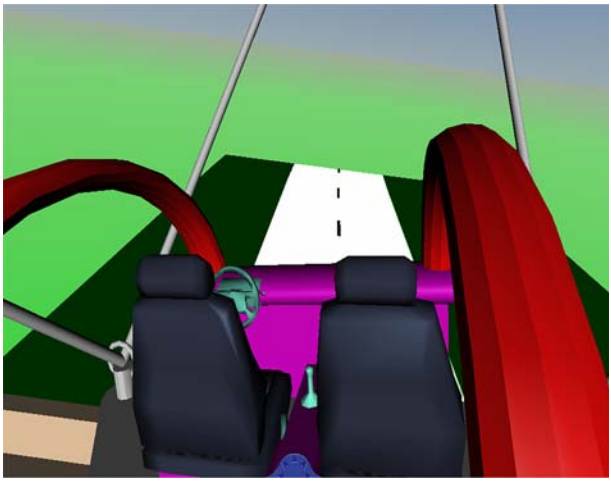

Fig. 4 View from the platform

3 Vehicle Simulation System (VSS) Dynamics

The platform end-effector of the cable robot has six Cartesian degrees of freedom, so to describe the dynamics of the platform, six differential equations are required. Newton's Second Law gives three differential equations and the angular momentum rate of change law gives an additional three differential equations. A detailed derivation of those equations is given in the Appendix. The set of differential equations can be expressed in the following matrix form:

$$\mathbf{A}\,\ddot{\mathbf{x}} + \mathbf{B}\,\dot{\mathbf{x}} = \begin{Bmatrix} \mathbf{F_R} \\ \mathbf{M_R} \end{Bmatrix} \tag{1}$$

where

$$\mathbf{A} = \begin{bmatrix} m \cdot \mathbf{1}_{3\times 3} & -m\,{}^0_2\mathbf{R}\,{}^2(\boldsymbol{\rho}_C)^{\otimes} \\ m\left({}^0_2\mathbf{R}\,{}^2\boldsymbol{\rho}_C\right)^{\otimes} & {}^0_2\mathbf{R}\,{}^2\mathbf{I}_{D(3\times 3)} \end{bmatrix}_{6\times 6} \quad \mathbf{B} = \begin{bmatrix} [\mathbf{0}]_{3\times 3} & -m\,{}^0_2\mathbf{R}\,{}^2(\boldsymbol{\omega}\times\boldsymbol{\rho}_C)^{\otimes} \\ [\mathbf{0}]_{3\times 3} & -{}^0_2\mathbf{R}\left({}^2\mathbf{I}^2_{D(3\times 3)}\boldsymbol{\omega}\right)^{\otimes} \end{bmatrix}_{6\times 6}$$

$$\begin{bmatrix} \mathbf{F}_{\mathrm{R}} \\ \mathbf{M}_{\mathrm{R}} \end{bmatrix} = \begin{bmatrix} {}^0\mathbf{F}_{\mathrm{ext}} + m\,{}^0\mathbf{g} + \sum\limits_{(i)} \left(-{}^0\hat{\mathbf{L}}_i\right) t_i \\ {}^0\mathbf{M}_{\mathrm{ext}} + {}^0\left(\mathbf{b}_M \times \mathbf{F}_{\mathrm{ext}}\right) + \sum\limits_{(i)} {}^0\mathbf{b}_i \times \left(-{}^0\hat{\mathbf{L}}_i\right) t_i + {}^0\,\boldsymbol{\rho}_C \times m\,{}^0\mathbf{g} \end{bmatrix}_{6\times 1}$$

and vector $\dot{\mathbf{x}} = \left[\dot{x}_D\ \dot{y}_D\ \dot{z}_D\ \omega_{x2}\ \omega_{y2}\ \omega_{z2}\right]^T$ is the velocity vector, or in a symbolic form $\dot{\mathbf{x}} = \begin{bmatrix} {}^0\vec{v}_D \\ {}^2\vec{\omega} \end{bmatrix}$, m is the platform mass, $\mathbf{1}_{3\times 3}$ denotes a 3×3 identity matrix, ${}^2\mathrm{I}_{D(3\times 3)}$ denotes the 3×3 platform inertia matrix, the symbol ⊗ denotes the matrix form of the cross product, ${}^0_2\mathbf{R}$ denotes the rotational matrix giving the orientation of the moving platform frame {2} with respect to the world frame {0}, and $\mathbf{F_R}$ and $\mathbf{M_R}$ are the resultant force and moment vectors acting externally on the platform.

A suitable way to solve the set of the VSS dynamics equations is to use the numerical solver of Matlab. A complex set of dynamics equations can be solved by the Matlab SimMechanics toolbox. However, the software cannot solve parallel cable-robot structure dynamics equations. Because of this limitation of the software, the set of equations has been solved using SimMechanics combined with additional programming in *m*-files. The iterative procedure of solving the cable robot equations is shown in Fig. 5.

The dynamics Eq. 1 and the numerical approach for their solution have been used to analyze the robot's workspace.

4 Vehicle Simulation System (VSS) Workspace

The workspace of the VSS is a set of points in 3D space that the VSS platform center of gravity can reach undergoing any positive cable tensions combination with maximum cable tension less than certain predefined value, i.e.:

$$\max_i t_i < t_{\mathrm{allowed}} \tag{2}$$

where t_{allowed} is the maximum allowed cable tension considering the limitation of the motors torques and the cables strength. The cable tensions depend on static forces such as weight and also on inertial forces:

$$t_i = t_i^{\mathrm{static}} + t_i^{\mathrm{dynamic}} \tag{3}$$

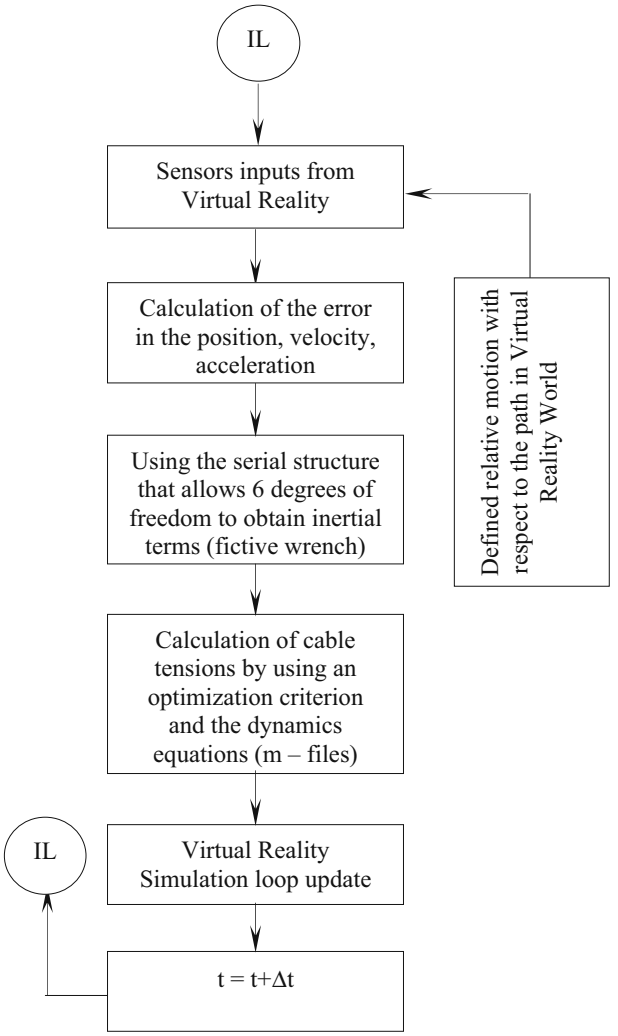

Fig. 5 The program iteration loop structure

While the cable tensions due to static forces depend only on the VSS position and orientation, the part of the cable tensions due to inertial forces depends on the VSS position and orientation and the robot motion through the workspace. In the case that inertial forces can be neglected comparing to static forces $t_i^{\text{static}} \gg t_i^{\text{dynamic}}$ the workspace of the robot can be uniquely determined in 3D space. Otherwise, the workspace depends on the robot trajectories, i.e., a radius of curvature, velocity and acceleration, and cannot be uniquely defined as a function of 3D coordinates. The approach of solving this problem of the workspace determination is that the workspace is analyzed due to static forces, and then the inertial forces contribution significance is analyzed separately.

4.1 Pseudostatic Workspace

The term pseudostatic means that cable tensions are analyzed for the robot in motion, from a point to a point perspective, but only static forces are considered. Using the right-hand

side of Eq. 1, and setting the left hand-side of the equation equal to zero, an equation for calculation of the cable tensions due to static load of the robot can be obtained:

$$\begin{bmatrix} {}^0\mathbf{F}_{\text{ext}} + m^0\mathbf{g} + \sum_{(i)} \left(-{}^0\hat{\mathbf{L}}_i\right) t_i \\ {}^1\mathbf{M}_{\text{ext}} + {}^1\left(\mathbf{b}_M \times \mathbf{F}_{\text{ext}}\right) + \sum_{(i)} {}^1\mathbf{b}_i \times \left(-{}^1\hat{\mathbf{L}}_i\right) t_i \end{bmatrix}_{6\times 1} = \begin{bmatrix} 0 \\ 0 \\ 0 \\ 0 \\ 0 \\ 0 \end{bmatrix} \tag{4}$$

In order to determine the VSS pseudostatic workspace, Eq. 4 is solved numerically for the cable tensions at a number of finite workspace volume pieces. Based on Eq. 4 and the optimization method that produces a minimum sum of positive cable tensions, the results are shown in Fig. 6.

The 3D domain divided into finite volume pieces is the prismatic space denoted by the edge lines of the prism with the ceiling triangular base. It can be noted that the maximum cable tensions appear when the platform approaches the top level triangular base. In this plane, six motors are planar with the platform and the theoretical value for the cable tensions is infinite.

The prismatic space that was considered is not filled completely in the figure. This means that wherever there is no marked box the cable tensions has maximum value greater than a predefined value, in this case 9,929 N, or there is no combination of positive cable tensions that will keep the platform at a given position and orientation. For this analysis in Fig. 6, the translation of the VSS platform is considered only, meaning all rotation angles are zeros.

The next case (Fig. 7) takes into account the translation and rotation of the VSS platform and calculations of the maximum cable tension allowing the rotation angles (three Euler's angles) within the range ±20°. The figure shows that the workspace is significantly reduced if rotation angles in the range [−20°, +20°] are allowed on all three axes. The workspace determination is done similarly to the previous case. However, in this case the angle range for all three angles is divided into a number of finite pieces also. The maximum cable tension at each position is calculated for each combination of the three angles within the

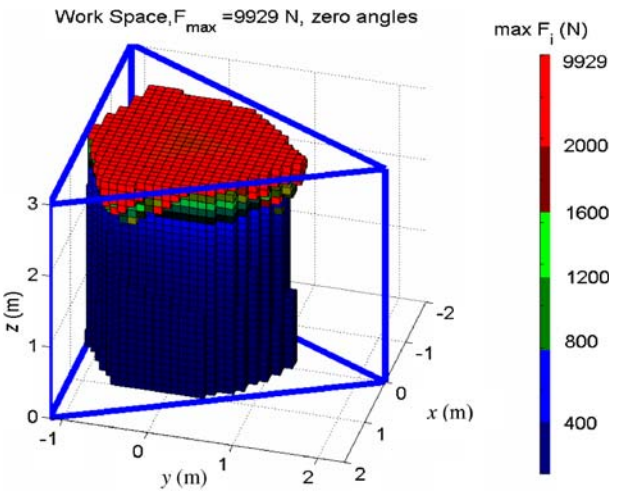

Fig. 6 Pseudo-static workspace for the zero angles (platform translation only)

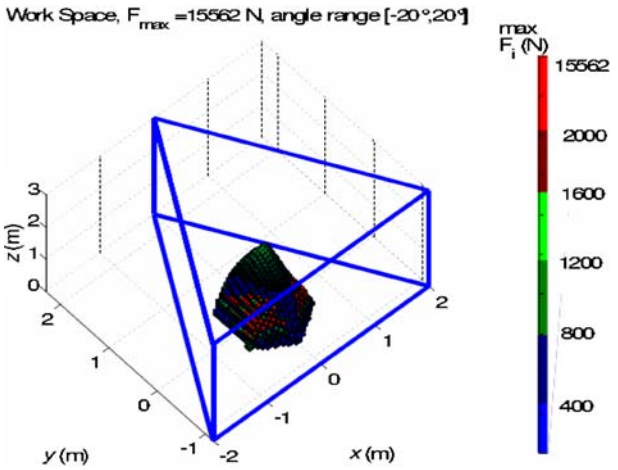

Fig. 7 VSS workspace for [−20°, 20°] rotation angles range on all axes

range [−20°, +20°]. If the overall cable tension for possible combinations is less than predefined limiting cable tension, then that position in 3D domain is considered as a part of the workspace, otherwise is out of the workspace. Further increase of the allowed rotation angles rapidly reduces the workspace size.

The workspace determination is important in order to limit planned robot trajectories onto the feasible pseudostatic workspace and to avoid high cable tensions that could be unsafe and damaging. If a planned robot trajectory is a subset of pseudostatic workspace and the inertial forces are not significant with respect to static forces, then cable tensions will be limited by a predefined maximum value.

This section addressed the pseudo-static workspace and showed that there is significant influence of the platform orientation onto the cable tensions. If even a relatively small angle range is allowed, this has as a consequence a significant workspace reduction. It has been shown that for the range [−20°, 20°] the reduction of the workspace is about 2/3. The significance of inertial forces on the cable tensions and workspace distortion will be discussed in the next section.

4.2 Inertial Forces Contribution to the VSS Cable Tensions

The cable robot platform trajectory can contain a number of segments that have small radii of curvature. Passing through those segments, the platform undergoes high inertial forces. These inertial forces, in general, can reduce the effective cable robot workspace. The influence of the inertial forces is shown in Fig. 8, for translational-only trajectories within the pseudostatic workspace of Fig. 6. The red color denotes the segments of the path with high cable tensions.

The analysis of the available cable robot workspace is necessary to make appropriate control design specifications and to constrain the control goals discussed in the next section.

5 Vehicle Simulation System (VSS) Control

The main goal of cable robot control is to obtain a specified position and orientation of the end-effector with respect to time. Besides this general goal of a cable robot control, in the

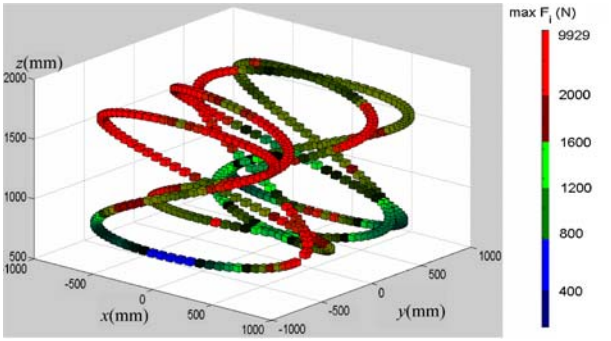

Fig. 8 Influence of inertial forces on the cable tensions

case of the VSS robot, there is an additional specific goal, the control of the platform end-effector acceleration in two directions and two angular accelerations about those two directions. The complexity of a cable robot control is reflected in the fact that a cable cannot push a body, and this fact requires establishment of significant restrictions on the controller outputs. Moreover, complexity added by non-linear kinematics and dynamics equations. The position, velocity and acceleration of the platform is specified in the Cartesian coordinate system, but the directly-controlled and directly-sensed variables are cable lengths. Indirectly controlled outputs are three positions of the platform center of gravity and three angles of the platform. This indirect control requires a non-linear transformation of coordinates.

When a classical control algorithm is applied, a local linearization has to be applied at each time step. This linearization process causes control errors that depend on the amount of non-linearity of variables trajectories, the time step, magnitudes of the velocity and acceleration. Because of those significant obstacles, in this work, classical control algorithms are applied in a combination with Fuzzy logic control algorithms. Besides this, a neural network controller has been tested.

Fuzzy logic control concept is successful in the area of non-linear systems control [2]. One disadvantage of this concept is high requirement for processing power that rapidly rises with the number of the fuzzy rules used by the control algorithm. In attempt to improve the robot control neural network control algorithms have also been tested. The controller architecture combining fuzzy logic control with classical control loops is discussed in the following sections.

5.1 Side Acceleration Control

In order to produce inertial forces that are sensed by a user of the VSS, the side acceleration has to be controlled. Figure 9 shows the Matlab/Simulink realization of the side acceleration control system.

The side acceleration control loop has a form of a cascade control consisting of a fuzzy logic controller and a classical control loop. The main (outer) control loop includes the fuzzy logic controller. The internal structure of the controller is shown in Fig. 10. Each input variable is associated with five membership functions. Membership functions for the first input variable are shown in Fig. 11. Controller inputs are: the radius of the desired trajectory “Rkinv”, the current side position of the robot platform “ypos” and an additional input that bears the information on whether a boundary is reached.

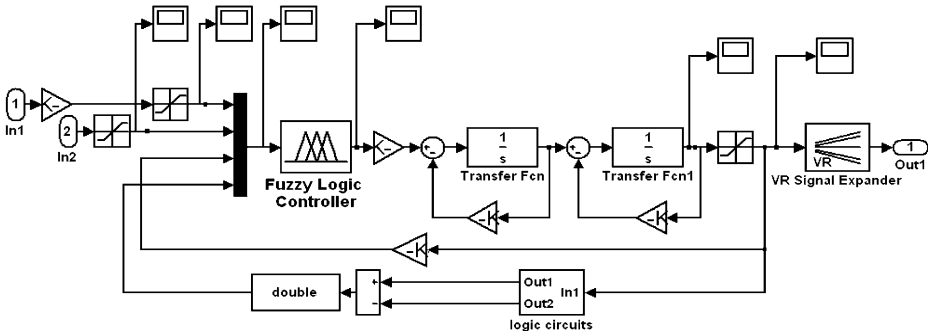

Fig. 9 Fuzzy logic control of the roll angle

The radius of curvature of a path becomes infinitely high for straight segments. In order to eliminate appearance of high values of this input variable, the inverse of the radius has been used. Membership functions associated with this input are: highly negative (trapezoidal form), low negative (triangular form), about zero (triangular form), low positive (triangular form), and highly positive (trapezoidal form). The second variable (the Cartesian feedback from the output) is associated with five membership functions in similar fashion as for the radius of the curvature. Simulation results show a high degree of control performance of this cascade control. Figure 12 shows an instant of the simulation during a side acceleration of the platform.

The main obstacle of the side acceleration control is the limited space of the cable robot motion. Often a side acceleration of significant duration is required for various vehicle simulation trajectories. The VSS can produce this acceleration but only in limited space. When a boundary is approached, the controller returns the platform slowly to the neutral position (below the human's capacity for detection) while maintaining the required side acceleration.

To make the simulation more realistic to a user, an additional effect has been introduced, the roll angle change to complement the side acceleration of the platform.

5.2 Roll Angle Control

In order to alleviate the influence of high inertial forces onto the driver and to make the simulation more realistic, it is necessary to change the roll angle (about the longitudinal axis) in such way that the resulting force, consisting of the gravity force and the inertial

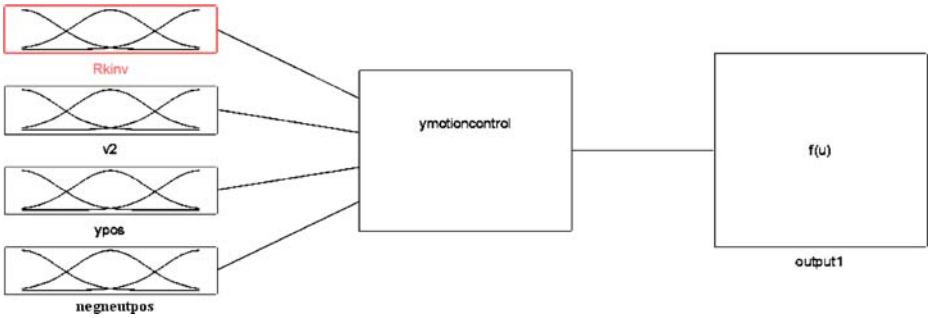

Fig. 10 Structure of the fuzzy logic controller for the side acceleration control

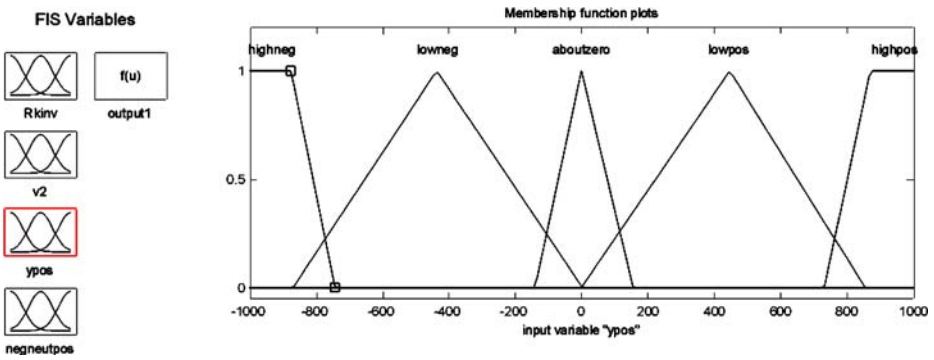

Fig. 11 Membership functions associated with the inverse radius of the curvature

force vector, acts perpendicularly to the seat. Similarly, an aircraft changes its direction motion with change of the roll angle toward the center of the curvature. The control loop for the roll angle is shown in Fig. 13.

The controller changes the roll angle depending on the side acceleration of the platform. Therefore, inputs into the control loop are the radius of curvature and the velocity of the desired vehicle trajectory. The input signals have noise, which cause errors in the derivatives of those signals. Because of this fact, the input signals are filtered, and output signals after the differentiation are limited to certain reasonable values.

Figure 12 shows an instant of the motion simulation during a side acceleration of the platform. The side acceleration is oriented to the left and consequently the inclination is to the left. The simulation results show that the applied controller satisfies the requirements, taking into consideration that the angle range is limited to [−20°, 20°] due to the fact that the available robot workspace reduces significantly with increasing the angle beyond this range.

Besides the side acceleration, the vehicle acceleration can also have a longitudinal component. The control concept of the longitudinal acceleration of the robot platform is discussed next.

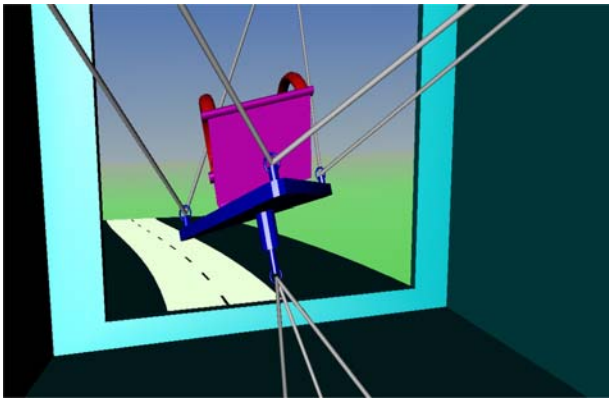

Fig. 12 Roll angle during a side acceleration of the robot platform

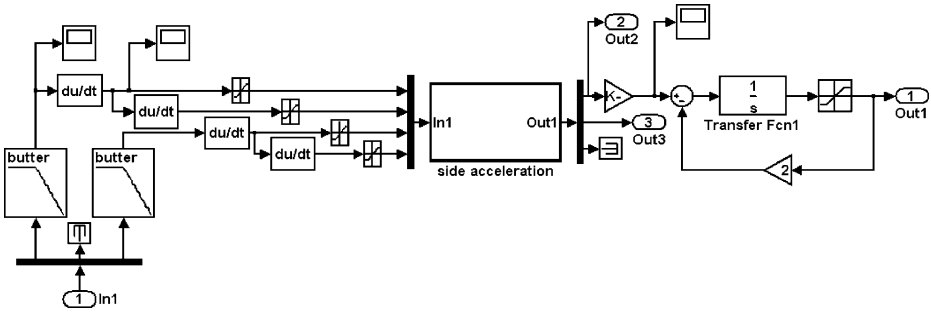

Fig. 13 Block diagram of the side acceleration control system

5.3 Longitudinal Acceleration Control

The purpose of the longitudinal acceleration control is to produce an adequate longitudinal acceleration of the robot platform, proportional to the acceleration of the simulated vehicle motion. The control loop for the longitudinal acceleration is shown in Fig. 14, with a structure similar to side acceleration control. The cascade control contains a fuzzy logic controller in the outer loop and two inner classical control loops. Input variables are associated with five membership functions each. The internal structure and the membership functions for the first input variable are shown in Figs. 15 and 16, respectively. The result of the simulation show satisfactory performance of this cascade control loop. An instant of the simulation is shown in Fig. 17.

The control loop in the following section shares the same input variable in order to provide adequate pitch angle of the platform.

5.4 Pitch Angle Control

The purpose of the pitch angle control is to provide the user with an additional effect that makes longitudinal acceleration realistic. The angle magnitude depends on the magnitude of the tangential acceleration, but it is limited to a range of [−20°, 20°] due to limited workspace of the robot. Figure 18 shows the control loop realized using Matlab/Simulink.

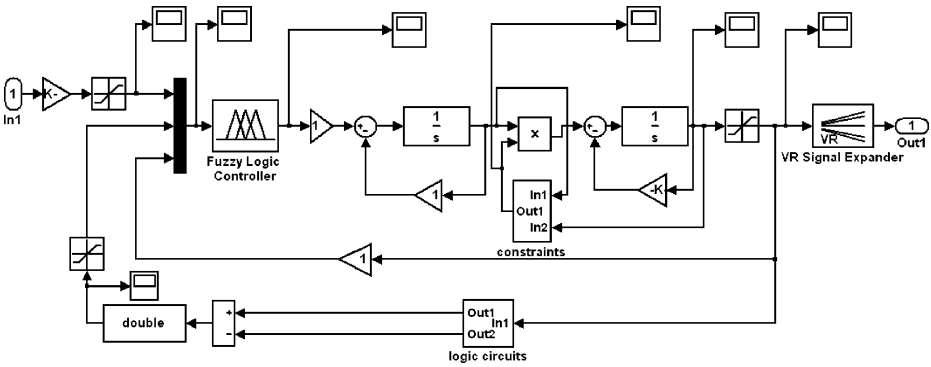

Fig. 14 Longitudinal acceleration control-loop

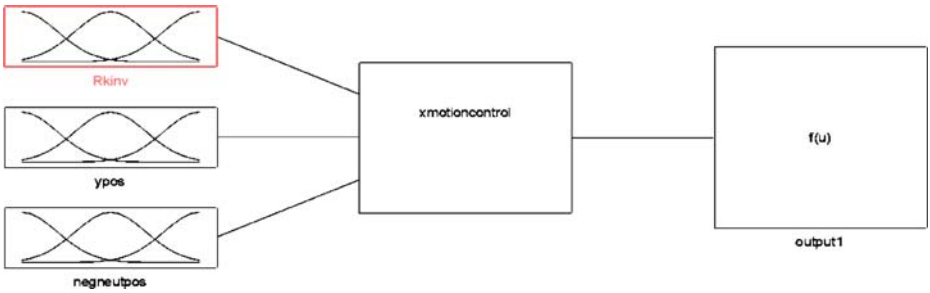

Fig. 15 Fuzzy logic controller structure for the longitudinal acceleration

The input signal bears information about the two components of the vehicle velocity (in the two horizontal directions), with high noise that causes significant problems with differentiation. Because of this problem, input signal is filtered, differentiated, again filtered and limited to a reasonable values. In the case of pitch angle control, classical control has been applied.

The results of the simulation (snapshot shown in Fig. 17) show that the control system has met the goals specified by the control design.

5.5 Cable Tensions Optimization Procedure

This section presents the method to maintain positive cable tensions for all commanded motions. The dynamic Eq. 1 can be used to calculate cable tensions t_i (i=1,…,9) necessary to produce a desired (known) acceleration of the platform. This under-constrained set of equations can be written in the following form:

$$\mathrm{Jac}_{6\times 9} \times \mathrm{t}_{9\times 1} = \mathrm{d}_{6\times 1} \tag{5}$$

To close the set of equations, we form a new set of constraints that ensure a minimization of the norm:

$$\left\|\mathbf{Jac}_{6\times 9} \times \mathbf{t}_{9\times 1} - \mathbf{d}_{6\times 1}\right\| \tag{6}$$

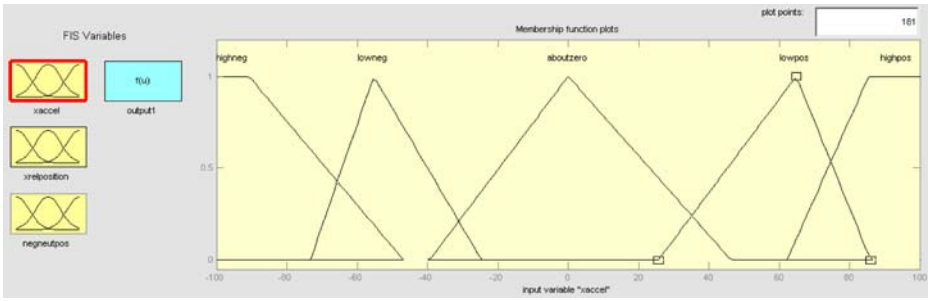

Fig. 16 Membership functions associated with the desired longitudinal acceleration

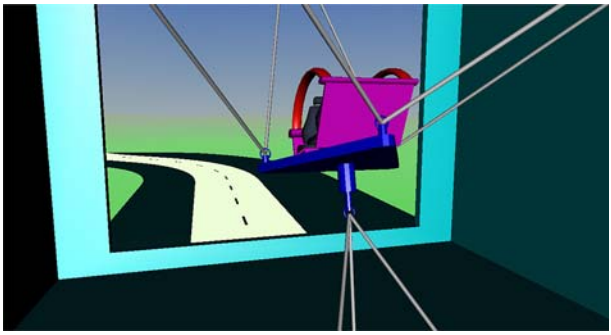

Fig. 17 Longitudinal acceleration control

in the following form:

$$\frac{\partial}{\partial t_i}\|\mathbf{Jac}_{6\times 9}\times \mathbf{t}_{9\times 1}-\mathbf{d}_{6\times 1}\|=0,\ i=1,\ldots \tag{7}$$

The additional constraints in the form of inequalities $t_i \geq 0$, $i=1,\ldots 9$, ensure that calculated values for the cable tensions are positive. Equation 7 can be solved numerically through an iterative procedure, without finding analytical expression for the derivatives. In a case that the platform crosses the boundaries of the available robot workspace, two potential problem situations appear: there is no solution for Eq. 7 without negative calculated cable tensions, or some calculated cable tensions are too high according to available cable materials and the motors maximum torque.

6 Combined Motion Control Simulation

In this section we simulate the vehicle simulation system control with side acceleration/roll angle control combined with longitudinal acceleration/pitch angle control for a representative simulated automotive vehicle motion, whose filtered acceleration commands are shown in Fig. 19.

Figures 20 show the six Cartesian motion variables, Fig. 21 the required cable lengths, and Fig. 22 the associated cable tensions for the simulated motion. The base and platform Cartesian coordinate frames, plus the cable numbering convention, was shown in Fig. 2. The three Cartesian angles α, β, and γ are rotations about the fixed X_B, Y_B, and Z_B axes, respectively.

The fuzzy logic controller for longitudinal acceleration gives a signal with relatively high magnitude at beginning of the simulation interval and after achieving a certain velocity of the simulated vehicle, the signal attenuates. The fuzzy logic controller for side

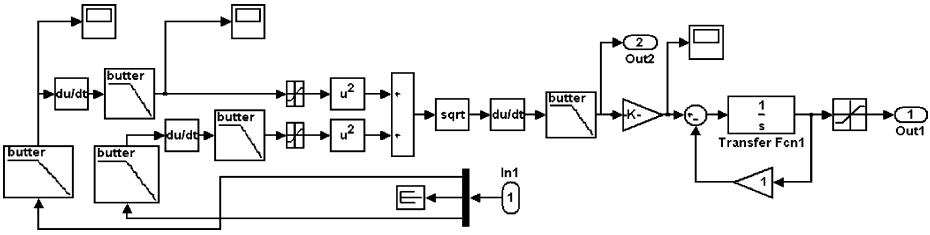

Fig. 18 Pitch angle control

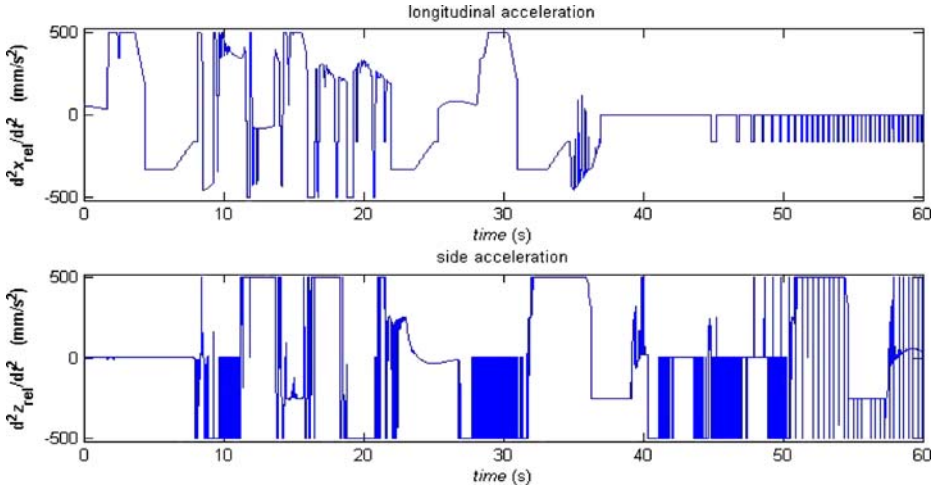

Fig. 19 Commanded longitudinal and side accelerations

acceleration changes the output signal very frequently in certain intervals. However, this signal is filtered before its application. The second lever of filtering is the filtering by the controlled object, i.e., the robot platform acts as an integrator block.

During the simulation, the pitch angle has been limited to [−15°, 15°] and the roll angle has been limited to [−20°, 20°] in order to avoid the further reduction of the available workspace. The robot platform height has been fixed to 1,200 mm, and the yaw angle to zero, as required by the motion nature of the vehicle that has been simulated.

Figures 21 and 22 show that whenever there is a sharp change in a cable length a corresponding cable tension reaches very high values. This fact restricts the desired path

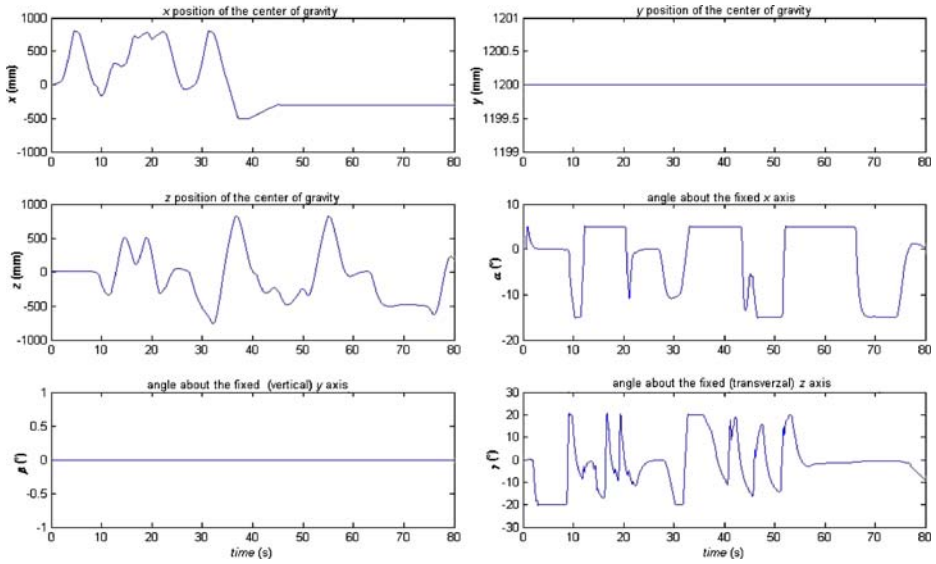

Fig. 20 Cartesian platform pose motion in combined simulation

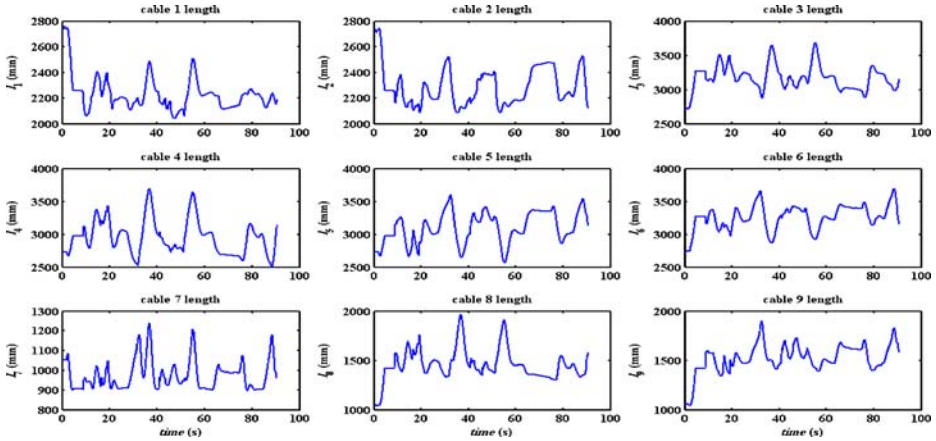

Fig. 21 Cable lengths in combined simulation

and motion created using virtual reality approach. The desired motion is created and written in a program, and can describe unfeasible motion requiring extremely high cable tensions and possibly violating the available workspace. Crossing the workspace boundaries would cause sudden drop of a control performance and possibly damage the system. The simulation phase is necessary before the real application for safety.

7 Conclusion

A cable-suspended vehicle simulation system has been introduced. The nonlinear dynamics equations were derived and the robot workspace was determined. Matlab/Simulink/SimMechanics/VR toolbox simulations were performed to test the developed hybrid fuzzy logic/classical controllers for side acceleration/roll angle control and also for longitudinal/pitch angle control.

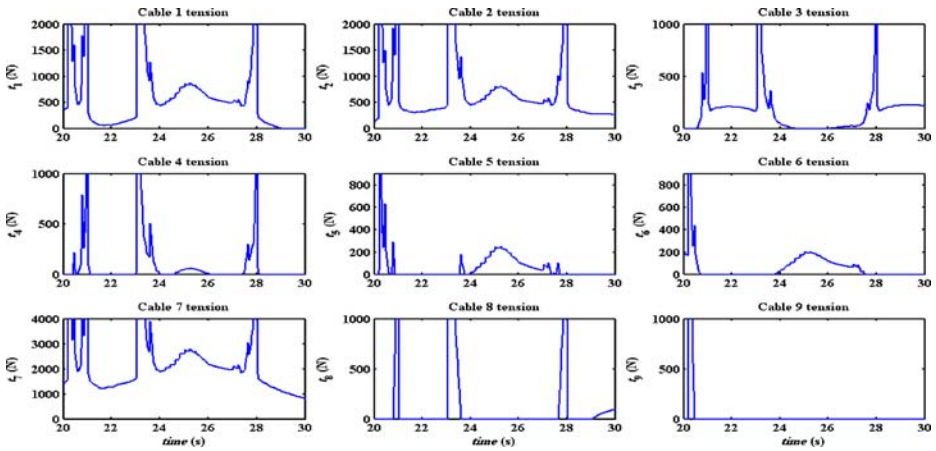

Fig. 22 Cable tensions in combined simulation

Fuzzy logic control shows high performance in simulations. To alleviate the discontinuities in the fuzzy logic controller output and to reduce the complexity of the controller (number of if-then rules and the number of input variables), the fuzzy logic controller can be combined in a cascade fashion with a classical control concept controller.

Neural network controllers have great advantage in controller processing speed, but the main disadvantage is that there is no guarantee for stability which eliminates the neural network control concept from this application.

In order to make valid control design specifications, a detailed dynamics and kinematics analysis of the robot has to be done. An important part of the analysis that precedes the controller design is the robot workspace analysis. The results of the workspace analysis showed that the size of the cable robot workspace is influenced by the platform angle change. For example, allowing angles to change within interval [−20°, 20°] reduces the workspace by approximately 66%. The available size of the cable robot workspace is influenced also by inertial forces acting on the platform.

Beside the constraints on angles change, restrictions must also be established for rates of change of cable lengths. To predict dangerous negative or high cable tensions, a simulation phase is necessary before an application on real system.

Future plans include implementation of the design and control for the whole-body haptics vehicle simulation system in hardware.

Appendix

Derivation of the Cable Robot Dynamics Equations

Figure 23 shows the free-body diagram for the vehicle simulation system. The moving frame is attached to a point different than the center of gravity, in general.

Newton's second law expressed in the coordinate frame {0} gives:

$$m\,\vec{a}_C = m\,\vec{g} + \sum_{(i)} \left(-\hat{\mathbf{L}}_i\right) t_i + \vec{F}_{\text{ext}} \tag{8}$$

where $\hat{\mathbf{L}}_i$ is the unit vector with direction of the ith cable (from point A_i to point B_i), t_i is the ith cable tension, $\vec{F}_{\text{ext}}$ is the external force. Acceleration of the center of gravity is evaluated using the acceleration of point D:

$${}^0\vec{a}_C = {}^0\vec{a}_D + {}^0\left(\vec{a} \times \vec{\rho}_C\right) + {}^0\vec{\omega} \times {}^0\left(\vec{\omega} \times \vec{\rho}_C\right) \tag{9}$$

or in the following form:

$${}^0\vec{a}_C = {}^0\vec{a}_D + \left(-{}^0\left(\vec{\rho}_C\right)^{\otimes}\right) \times {}^0\dot{\vec{\omega}} + \left(-{}^0\left(\vec{\omega} \times \vec{\rho}_C\right)^{\otimes}\right) \times {}^0\vec{\omega} \tag{10}$$

where the superscript 0 denotes that a vector is expressed within coordinate frame {0} and the symbol ⊗ denotes the matrix form of the cross product. The angular momentum rate of change law expressed in coordinate frame {1} gives:

$$\frac{\mathrm{d}}{\mathrm{d}t}\vec{H}_C = \vec{M}_{\text{ext}} + \left(\vec{b}_M - \vec{\rho}_C\right) \times \vec{F}_{\text{ext}} + \sum_{(i)} \left(\vec{b}_i - \vec{\rho}_C\right) \times \left(-\hat{L}_i\right) t_i \tag{11}$$

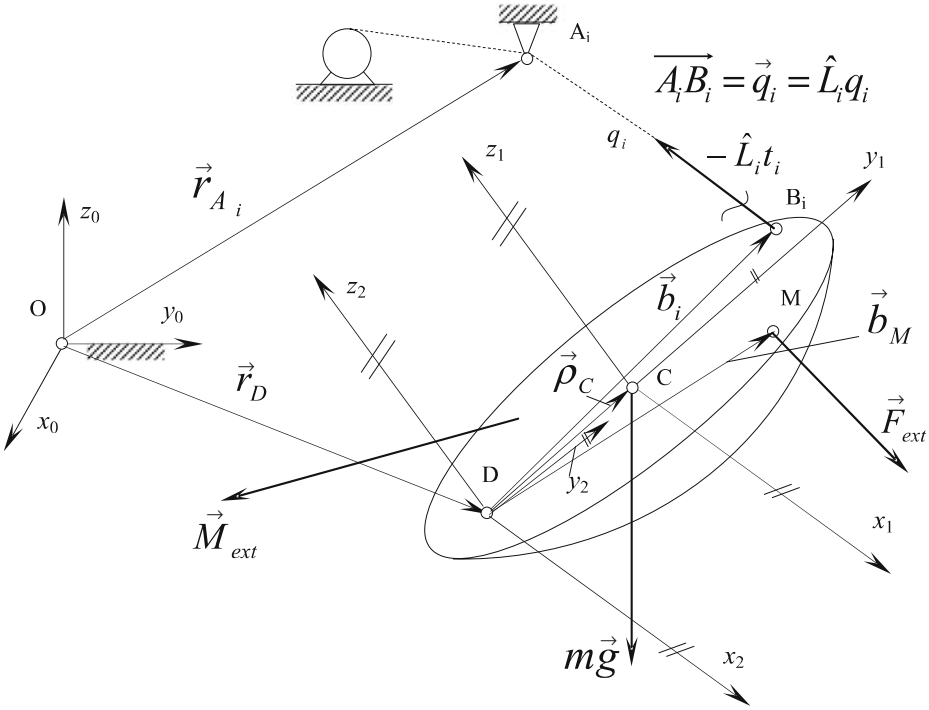

Fig. 23 Moving coordinate frame attached at a point different from center of mass

The left hand-side of Eq. 11 can be expressed in the following form:

$$\frac{\mathrm{d}}{\mathrm{d}t}{}^1\vec{H}_C = \underbrace{\left(\frac{\mathrm{d}}{\mathrm{d}t}\left|\vec{H}_C\right|\right)\frac{{}^1\vec{H}_C}{\left|\vec{H}_C\right|}}_{\substack{\text{rate of change in intensity,}\\ \text{multiplied with unit vector}}} + \underbrace{\left({}^1\vec{\omega}\times{}^1\vec{H}_C\right)}_{\text{result of a direction change}} = \tag{12}$$

$${}^1\mathbf{I}_C{}^1\dot{\vec{\omega}} + {}^1\vec{\omega}\times\left({}^1\mathbf{I}_C{}^1\vec{\omega}\right)$$

By inserting Eq. 12 into Eq. 11 the following can be obtained:

$$\begin{aligned} &{}^1\mathbf{I}_C^1\dot{\vec{\omega}} + {}^1\vec{\omega}\times\left({}^1\mathbf{I}_C^1\vec{\omega}\right) \\ &= {}^1\vec{M}_{\text{ext}} + {}^1\left(\vec{b}_M - \vec{\rho}_C\right)\times{}^1\vec{F}_{\text{ext}} + \sum_{(i)}{}^1\left(\vec{b}_i - \vec{\rho}_C\right)\times{}^1\left(-\hat{L}_i\right)t_i \end{aligned} \tag{13}$$

where the superscript 1 denotes that a vector or matrix is expressed within coordinate frame {1}. We transform each term in Eq. 13 to be expressed within coordinate frame {2}.

The angular momentum change law is valid for center of mass, not for the point D, but we can use D'Alembert's principle to transform those moments onto the point D. The inertial moment $\vec{M}^{\text{inert}}$ is:

$$-\frac{\mathrm{d}}{\mathrm{d}t}\vec{H}_C = \vec{M}^{\text{inert}} \tag{14}$$

and the inertial force $\vec{F}^{\text{inert}}$ is:

$$-m\vec{a}_C = \vec{F}^{\text{inert}} \tag{15}$$

A moment is free vector and we can move the inertial moment to the point D, but a force produces moment $\vec{\rho}_C \times \vec{F}^{\text{inert}}$. The equation for rotational motion, expressed in coordinate frame {1}, according to D'Alembert's principle, is:

$$-\vec{M}^{\text{inert}} - \vec{\rho}_C \times \vec{F}^{\text{inert}} = \vec{M}_{\text{ext}} + \vec{b}_M \times \vec{F}_{\text{ext}} + \sum_{(i)} \vec{b}_i \times \left(-\hat{L}_i\right) t_i + \vec{\rho}_C \times m\vec{g} \tag{16}$$

After substitution of the terms in Eq. 16 following can be obtained:

$$\begin{aligned} &\mathbf{I}_C \dot{\vec{\omega}} + \vec{\omega} \times \left(\mathbf{I}_C \vec{\omega}\right) + m\vec{\rho}_C \times \left(\vec{a}_D + \dot{\vec{\omega}} \times \vec{\rho}_C + \vec{\omega} \times \left(\vec{\omega} \times \vec{\rho}_C\right)\right) \\ &= \vec{M}_{ext} + \vec{b}_M \times \vec{F}_{\text{ext}} + \sum_{(i)} \vec{b}_i \times \left(-\hat{L}_i\right) t_i + \vec{\rho}_C \times m\vec{g}, \end{aligned} \tag{17}$$

where:

$$\mathbf{I}_C = \mathbf{I}_D - m \begin{bmatrix} y_{1D}^2 + z_{1D}^2 & -x_{1D}y_{1D} & -x_{1D}z_{1D} \\ -x_{1D}y_{1D} & x_{1D}^2 + z_{1D}^2 & -y_{1D}z_{1D} \\ -x_{1D}z_{1D} & -y_{1D}z_{1D} & x_{1D}^2 + y_{1D}^2 \end{bmatrix} = \mathbf{I}_D - \Delta\mathbf{I} \tag{18}$$

$$\vec{\rho}_C \times \left(\dot{\vec{\omega}} \times \vec{\rho}_C\right) = \dot{\vec{\omega}}\left(\rho_C^2\right) - \vec{\rho}_C\left(\dot{\vec{\omega}} \times \vec{\rho}_C\right) \tag{19}$$

$$\begin{aligned} \vec{\rho}_C \times \left(\vec{\omega} \times \left(\vec{\omega} \times \vec{\rho}\right)\right) &= \vec{\rho}_C \times \left(\vec{\omega}\left(\vec{\omega} \times \vec{\rho}_C\right) - \vec{\rho}_C\left(\omega^2\right)\right) \\ &= \left(\vec{\rho}_C \times \vec{\omega}\right)\left(\vec{\omega} \times \vec{\rho}_C\right) \end{aligned} \tag{20}$$

After substituting Eqs. 18, 19 and 20 into Eq. 17, the following form expressed in coordinate frame {2} can be obtained:

$$\mathbf{I}_D \dot{\vec{\omega}} + \vec{\omega} \times \left(\mathbf{I}_D \vec{\omega}\right) + m\vec{\rho}_C \times \vec{a}_D = \vec{M}_{\text{ext}} + \vec{b}_M \times \vec{F}_{\text{ext}} + \sum_{(i)} \vec{b}_i \times \left(-\hat{L}_i\right) t_i + \vec{\rho}_C \times m\vec{g} \tag{21}$$

Equations 8 and 21 can be written in the following form:

$$\begin{bmatrix} m \times \mathbf{1}_{3\times3} & -m\,{}^0_2\mathbf{R}\,{}^2(\boldsymbol{\rho}_C)^{\otimes} \\ m\left({}^0_2\mathbf{R}\,{}^2\boldsymbol{\rho}_C\right)^{\otimes} & {}^0_2\mathbf{R}\,{}^2\mathbf{I}_{D(3\times3)} \end{bmatrix}_{6\times6} \ddot{\mathbf{x}}_{6\times1} + \begin{bmatrix} [\mathbf{0}]_{3\times3} & -m\,{}^0_2\mathbf{R}\,{}^2(\boldsymbol{\omega}\times\boldsymbol{\rho}_C)^{\otimes} \\ [\mathbf{0}]_{3\times3} & -{}^0_2\mathbf{R}\left({}^2\mathbf{I}^2_{D(3\times3)}\boldsymbol{\omega}\right)^{\otimes} \end{bmatrix}_{6\times6} \dot{\mathbf{x}}_{6\times1}$$
$$= \begin{bmatrix} {}^0\mathbf{F}_{\text{ext}} + m\,{}^0\mathbf{g} + \sum_{(i)} \left(-{}^0\hat{L}_i\right) t_i \\ {}^0\mathbf{M}_{\text{ext}} + {}^0\left(\mathbf{b}_M \times \mathbf{F}_{\text{ext}}\right) + \sum_{(i)} {}^0\mathbf{b}_i \times \left(-{}^0\hat{L}_i\right) t_i + {}^0\,\boldsymbol{\rho}_C \times m\,{}^0\mathbf{g} \end{bmatrix}_{6\times1}, \tag{22}$$

Equation 22 can be expressed in the more compact form given in the text of this article in Eq. 1. This is the coupled nonlinear set of dynamics equations for the vehicle simulation system.

References

1. Albus, J.S., Bostelman, R., Dagalakis, N.G.: The NIST ROBOCRANE. J. Robot. Syst **10**, (5), 709–724 (1993)
2. Avdagic, Z.: Artificial Intelligence & Fuzzy-Neuro-genetic Algorithms. Grafoart, Sarajevo (2003) (in Bosnian)
3. Bosscher, P., Riechel, T.A., Ebert-Uphoff, I.: Wrench-feasible workspace generation for cable-driven robots. IEEE Trans. Robot. Autom **22**, (5), 890–902 (2006)
4. Marshall, T.: Aerial Cable Range, http://www.drdc-rddc.gc.ca/seco/msrr/view_e.asp?id = 189. Aberdeen Proving Ground, Maryland (2007)
5. Park, J., Chung, W., Moon, W.: Wire-suspended dynamical system: stability analysis by tension-closure. IEEE Trans. Robot. Autom **21**, (3), 298–308 (2005)
6. Pusey, J., Fattah, A., Agrawal, S., Messina, E.: Design and workspace analysis of a 6–6 cable-suspended parallel robot. Mech. Mach. Theory **39**, 761–778 (2004)
7. So-Ryeok, O., Agrawal, S.: Generation of feasible set points and control of a cable robot. IEEE Trans. Robot. Autom **22**, (3), 551–558 (2006a)
8. So-Ryeok, O., Agrawal, S.: A reference governor-based controller for a cable robot under input constraints. IEEE Trans. Control Syst. Technol **13**, (4), 639–645 (2006b)
9. Usher, K., Winstanley, G., Corke, P., Stauffacher, D.: A cable-array robot for air vehicle simulation. Proceedings of the 2004 Australasian Conference on Robotics & Automation, December 6–8. Canberra, Australia (2004).
10. Williams, R.L. II: Cable-suspended vehicle simulation system concept, CD. Proceedings of the ASME International Design Technical Conferences, 31st Mechanisms and Robotics Conference, Paper # DETC2007-34595, Las Vegas NV, September 4–7 (2007)
11. Williams II, R.L., Albus, J.S., Bostelman, R.: 3D cable-based Cartesian metrology system. J. Robot. Syst **21**, (5), 237–257 (2004)
12. Williams II, R.L., Gallina, P.: Translational planar cable-direct-driven robots. J. Intell. Robot. Syst **37**, 69–96 (2003)
13. Yingjie, L., Wenbai, Z., Gexue, R.: Feedback control of a cable-driven Gough–Stewart platform. IEEE Trans. Robot. Autom **22**, (1), 198–202 (2006)